Molecular Dynamics Simulations of H(2) Adsorption in Tetramethyl Ammonium Lithium Phthalocyanine Crystalline Structures

ARTICLE *in* THE JOURNAL OF PHYSICAL CHEMISTRY B · JANUARY 2009

Impact Factor: 3.3 · DOI: 10.1021/jp8050998 · Source: PubMed

Molecular Dynamics Simulations of H_2 Adsorption in Tetramethyl Ammonium Lithium Phthalocyanine Crystalline Structures

Kevin Lamonte,[†] Diego A. Gómez Gualdrón,[†] Fredy A. Cabrales-Navarro,[†] Lawrence G. Scanlon,[‡] Giselle Sandi,[§] William Feld,[||] and Perla B. Balbuena*,[†]

Department of Chemical Engineering, Texas A&M University, College Station, Texas 77843, Air Force Research Laboratory, Energy Storage &Thermal Sciences Branch, Wright-Patterson Air Force Base, Ohio 45433, Argonne National Laboratory, Chemistry Division, 9700 South Cass Avenue, Argonne, Illinois 60439, and Department of Chemistry, Wright State University, Dayton, Ohio 45435

Received: June 10, 2008; Revised Manuscript Received: September 23, 2008

Tetramethyl ammonium lithium phthalocyanine is explored as a potential material for storage of molecular hydrogen. Density functional theory calculations are used to investigate the molecular structure and the dimer conformation. Additional scans performed to determine the interactions of a H_2 molecule located at various distances from the molecular sites are used to generate a simple force field including dipole-induced-dipole interactions. This force field is employed in molecular dynamics simulations to calculate adsorption isotherms at various pressures. The regions of strongest adsorption are quantified as functions of temperature, pressure, and separation between molecules in the adsorbent phase, and compared to the regions of strongest binding energy as given by the proposed force field. It is found that the total adsorption could not be predicted only from the spatial distribution of the strongest binding energies; the available volume is the other contributing factor even if the volume includes regions of much lower binding energy. The results suggest that the complex anion is primarily involved in the adsorption process with molecular hydrogen, whereas the cation serves to provide access for hydrogen adsorption in both sides of the anion molecular plane, and spacing between the planes.

1. Introduction

Developing materials for hydrogen storage is a scientific and technological challenge. While a variety of materials are being currently analyzed both experimentally and computationally, the optimum material that could store hydrogen at room temperature and also is able to easily release it as needed has not been found yet. Carbon-based and metal hydride materials are the most popular and a variety of alternatives have been reviewed.[1] In recent work, we have studied corannulene[2] and Li-doped corannulene[3,4] and we found that the presence of the Li ions has two beneficial effects on H_2-storage: first is to separate the adsorbent molecules thus opening additional storage volume, and second there is a slight increase of the physisorption energy due to the Li−H_2 interactions. These findings motivated our new investigation of materials that may arrange in a layered structure where the layers may be more separated than graphite-type materials and where there is a distribution of charges that may induce additional electrostatic interactions on the H_2 molecules.[5] Specifically, the purpose of investigating a layered structure based on a phthalocyanine molecule is to take advantage of its relatively large surface area as compared with the cyclopentadienyl anion[5] but still maintaining dipole/induced-dipole interaction. For such system, it is the complex anion that is involved in the hydrogen adsorption process whereas the tetra-alkyl-ammonium cation serves the purpose of spacing the phthalocyanine rings in order to permit hydrogen adsorption to take place on both sides of the ring. The selected system is tetramethyl ammonium lithium phtalocyanine (TMA-LiPc) which has a calculated dipole moment of 14.23 D that contrasts with our previous investigation using corannulene as an adsorbent where van der Waals forces involved in the physisorption process are enhanced by a much smaller dipole of 2.15 D.[2]

Graphitic layers as represented by coronene have been investigated by ab initio calculations and are representative of weak van der Waals forces of interaction. Single crystal results for phthalocyanine-based materials such as MgPc and H_2Pc show that the ring separation is either 4.8 or 3.8 Å, respectively, and therefore at these separation distances hydrogen adsorption would be very minimal. LiPc would not be attractive since in this case the ring separation is 3.24 Å. Thus, a tetra-alkyl-ammonium cation has been used in order to ensure both sides of the phthalocyanine aromatic ring are available for hydrogen adsorption. In the case of dilithium phthalocyanine (Li_2Pc), the phthalocyanine rings are separated by 3.5 Å;[6] such narrow separation precludes adsorption of molecular hydrogen between the rings. We have found that Li_2Pc dried at 160 °C for the purpose of hydrogen storage measurements is an electronic conductor based on electrochemical characterization. This implies that ring separation is sufficiently close to allow electronic conduction but does not favor hydrogen adsorption between the rings. By converting Li_2Pc into tetra-butyl-ammonium lithium phthalocyanine (TBA-LiPc) electrochemical characterization has shown that TBA-LiPc is now an insulating material. Correspondingly, we have found that the number of hydrogen molecules adsorbed at 77 K and 45 bar increases from 10 for Li_2Pc to 24 for TBA-LiPc. In this investigation, we have used tetra-methyl-ammonium lithium phthalocyanine (TMA-

* To whom correspondence should be addressed. E-mail: balbuena@tamu.edu.
[†] Texas A&M University.
[‡] Wright-Patterson Air Force Base.
[§] Argonne National Laboratory.
[||] Wright State University.

10.1021/jp8050998 CCC: $40.75
Published on Web 11/12/2008

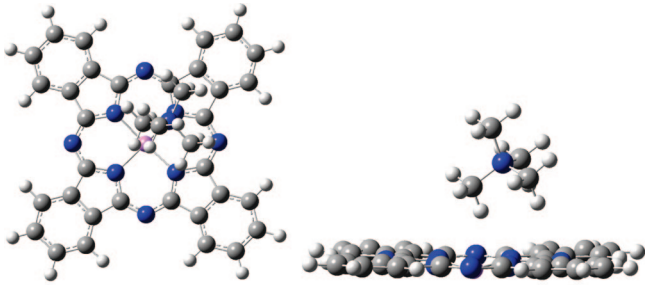

Figure 1. TMA-LiPc geometry optimized using B3LYP/6-31 g(d,p). These results along with those from the M05-2X/6-31 g(d, p) and B3LYP/6-31 g(d,p)++ are reported as Supporting Information.

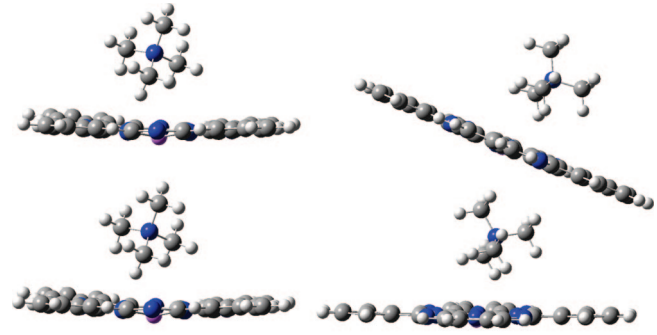

Figure 2. TMA-LiPc dimer optimized using B3LYP/6-31G(d,p). These results along with those from the M05-2X/6-31G(d,p) method are reported as Supporting Information.

LiPc) to determine the effect of a layered structure on the physisorption process via molecular dynamics simulations. In the case of χ-Li_2Pc[7] simulating the layered structure of the Li_2Pc test material, our (unpublished) MD results suggest at 300 K and 77 bar that 0.71 wt % H_2 is adsorbed versus experimentally 0.72 wt % H_2 is absorbed at 298 K and 77 bar.

We compute the interactions of molecular hydrogen with TMA-LiPc using density functional theory (DFT) and use the results to develop a force field for such interactions. Since the crystalline structure of TMA-LiPc is not known (to the best of our knowledge), we have assumed that these materials arrange in layered structures, based on the similarity of the molecule with other derivatives of phtalocyanine.[7] DFT calculations in dimers are utilized to obtain an estimate of the interlayer distance (ILD) and molecular dynamics (MD) simulations are then run on TMA-LiPc layered structures to estimate H_2 adsorption isotherms at 77, 177, 236, 273, and 300 K. Diffusion coefficients are also analyzed to investigate the strength of H_2 physisorption in these materials. We note that the predictive capability of the current method has been previously validated for adsorption of molecular hydrogen in corannulene stacks where experimentally the wt % hydrogen adsorbed is 0.8 wt % at 298 K and 72 bar. MD simulation of this adsorbent showed that 0.72 wt % hydrogen adsorbed at 300 K and 72 bar.[2]

2. Methods

2.1. Density Functional Theory Calculations. Density functional theory was used to optimize the geometry of a single molecule of TMA-LiPc; the energy optimization was performed using the Becke gradient-corrected exchange functional[8,9] in conjunction with the Lee−Yang−Parr correlation functional[10] with three parameters (B3LYP) and the 6-31 g(d,p) basis set; this molecular geometry (shown in Figure 1) was used in the MD simulations. Several studies have reported the lack of ability of some DFT functionals to compute weak dispersion interactions.[11−14] This effect should be less severe when polar interactions are added to dispersion forces, such as the case of TMA-LiPc. However, to assess this effect, we have evaluated the optimized geometries of the monomer and dimer using the M05-2X functional,[15] and the monomer geometry was also investigated using B3LYP with 6-31 g(d,p)++ to address the effect of added diffuse functions. The optimized structures and charge distribution do not differ significantly from that of the B3LYP/6-31 g(d,p) prediction. All the optimized structures are provided as Supporting Information. The rest of the manuscript refers to the results from the B3LYP/6-31 g(d,p) calculations.

The dipole moment computed with B3LYP/6-31 g(d,p) was 14.23 Debye and the volumetric polarizability was 631.08 $Bohr^3$ $= 9.352 \times 10^{-23}$ cm^3. The Mulliken charge distribution yielded molecular charges ranging from −0.614 to +0.406; the maximum values are in the inner ring carbon (positive) and nitrogen atoms (negative) on the phthalocyanine (Pc).

A dimer in stacked arrangement was also optimized. The initial and final configurations are shown in Figure 2. The initial distance between molecules was 8.36 Å. During optimization the two TMA-LiPc units separated slightly and the two Pc tilted to form an angle of about 36°. The final distance between the TMA cations was 8.24 Å and the average distance between corresponding atoms was 8.49 Å. Gaussian 03 set of programs[16] was used for all ab initio calculations.

2.2. Molecular Dynamics Simulations. ***2.2.1. Force Field Development.*** Following our previous studies of hydrogen storage, each diatomic hydrogen molecule was represented as a single site.[2] Due to the large TMA-LiPc dipole, a dipole may be induced on the hydrogen molecule as it approaches the molecule, thus the charge on each hydrogen atom depends on its proximity to TMA-LiPc. Therefore, the strength of the electrostatic interactions varies with the distance H_2-TMA-LiPc. However, we are representing the H_2 molecule with a single site, and even if a two-site model were used, the actual electrostatic interaction can hardly be described by assigning fixed charges to those sites which would remain constant during the simulation. Thus, we use a modified Lennard-Jones (LJ) potential which includes the potential energy due to dipole/induced-dipole interactions. The general formula for the mean potential energy due to dipole/induced-dipole interactions is

$$\overline{\Gamma}_{ij} = -\frac{(\alpha_i \mu_j^2 + \alpha_j \mu_i^2)}{(4\pi\varepsilon_0)^2 r_{ij}^{\ 6}} \tag{1}$$

where i refers to hydrogen and j to TMA-LiPc, α_k is the static molecular polarizability, and μ_k is the dipole moment of component k, and ε_o is the vacuum dielectric constant. To calculate the dipole induction of TMA-LiPc on H_2 we calculate the field strength around the former by means of

$$E = \frac{\mu}{\alpha} \tag{2}$$

An alternative expression of the polarizability in units of volume (cm^3) is given by: [17]

$$\alpha' = \frac{\alpha}{4\pi\varepsilon_0} \tag{3}$$

The volumetric polarizability for the hydrogen molecule (α') is reported in the literature as 8.10×10^{-25} cm^3.[18] Using the computed value of this property for TMA-LiPc as well as its dipole moment, the mean potential energy due to dipole/induced-dipole interactions between TMA-LiPc and H_2, eq 1, results in eq 4 with r given in Å

$$\overline{\Gamma}_{ij} = -\frac{1056250}{r_{ij}^{\ 6}}\text{meV} \tag{4}$$

However, if this correction were applied to all the TMA-LiPc atomic sites it would overestimate the dipole/induced dipole interaction strength, dramatically overestimating the adsorption energy. Thus, we postulate that such correction must be distributed among the sites of the macromolecule in such a way that adding the contributions of each site somehow reproduces the global effect. Further, the distribution of hydrogen around TMA-LiPc requires a dipole correction assigned on the basis of actual H_2/site interactions. Figure 3 shows the molecular charge distribution with atomic charges fitted to the electrostatic potential at selected points using the Merz−Singh−Kollman scheme.[19] At the left, the different zones of the molecule together with the net charge of each zone are illustrated. These zones were determined by grouping atoms with similar charges in each region. For instance, carbons that belong to "outer ring B" bear charges similar to those of the terminal hydrogen atoms, and there are two of these regions with identical net charge located diagonally opposed to each other with respect to the center of the anion. The cation is decomposed into the cation top and the cation bottom, whereas the anion is composed by 2 outer rings A, 2 outer rings B, and an inner ring. The inner ring is composed by N and C atoms with a positive lithium atom in the center. Figure 3 (right) shows the atoms colored according to their electrostatic potential-derived charges with the color scale shown in the bar. Notice that the charges are especially high in the inner ring while in the other anion zones the charges are negligible. The cation shows moderately high charges. Because of this charge distribution, as H_2 approaches each of the zones, different degrees of H_2 polarization may occur. To account for this behavior, we assigned weight factors to each site; these factors are used to modify the site−site Lennard-Jones pair potentials.

Figure 3 shows that some site charges have high absolute values and therefore highly negative or positive ESP values around them. For this reason we tried two approaches for the calculation of weight factors (w_i) that are used along with eq 4. In the first approach, weight factors are proportional to the values of the charges on the heavy atoms; in the second one the weight factors were calculated on the basis of an average induced dipole moment on H_2 corresponding to each site. Such dipole moment was obtained by averaging the results from single point DFT calculations performed as H_2 was approaching a specific TMA LiPc site varying the distance d' between the H_2 and the site. From 10 to 5 Å we used intervals of 1.0 Å, and intervals of 0.5 Å from 5 to 2.5 Å. A typical calculation path is illustrated in Figure 4 for the case of H_2 approaching the cation top along the red dashed line, moving in a stepwise manner as described above.

The results of H_2 uptake in an ensemble of TMA-LiPc molecules as calculated by MD simulations using parameters from both approaches are very similar; here we report only those corresponding to the second method. Values of the average induced dipole moment and calculated weight factors are shown in Table 1 for the different sites, where we have disregarded the contribution of hydrogen atoms in TMA-LiPc and we assigned weight factors only for the interactions of H_2 with the heavy atoms. The C atoms that belong to both the inner and an outer ring of the cation were also disregarded because of their almost zero charge. The induced dipoles were also calculated using the M05-2X functional, the results did not show significant variations, and are included in Table 1

Once the weight factors are calculated, the total potential energy for each *ij* pair (between an *i* site of the macromolecule and the *j* site representing the H_2 molecule) interaction is the sum of the Lennard-Jones potential and the corresponding weighted dipole correction (with C the constant in equation 4 given in proper units) as follows:

$$u(r_{ij}) = 4\varepsilon\left(\left(\frac{\sigma_{ij}}{r_{ij}}\right)^{12} - \left(\frac{\sigma_{ij}}{r_{ij}}\right)^{6}\right) - \frac{w_i C}{r_{ij}} \tag{5}$$

For the TMA-LiPc atoms, we used the LJ parameters in the original Dreiding force field reference,[20] and for the hydrogen molecule the spherical (single site) model with $\varepsilon/k = 34.2$ K and $\sigma = 2.96$ Å.[2] The Lorentz−Berthelot mixing rules[21] were applied. Once this total potential energy given by eq 5 is calculated for different r_{ij} distances from the hydrogen molecule (*j*) to the site *i*, new effective LJ parameters are calculated by fitting these values to a simple LJ potential (without the dipole/induced-dipole term). Figure 5 shows the resulting LJ curves and parameters for each H_2-TMA-LiPc site interaction.

A few TMA-LiPc atoms such as hydrogen atoms and some carbon atoms do not alter the dipole moment of H_2; therefore in our MD simulations their parameters are the original ones for the Dreiding force field.[20]

2.2.2. MD Procedure. MD simulations were performed in the canonical NVT ensemble, using Evans thermostat[22] to keep the temperature constant, using the DL_POLY program. [23] The unit cell contained 18 molecules of TMA-LiPc in a $3 \times 3 \times 2$ stacked cubic arrangement (Figure 6) and 770 H_2 molecules. In order to simulate the TMA-LiPc crystal structure, in addition to the interlayer distance (estimated from the dimer separation as 8.49 Å), an estimate of the intermolecular distance (IMD) is needed. The IMD is defined as the distance between the centers of the planes of two LiPc molecules located side by side, and it was estimated as 13.85Å, being equal to that of the Li_2Pc crystal structure that we reported recently.[7] To simulate higher pressures, the gas-phase volume was adjusted accordingly. After the simulation, the pressure in the gas-phase region was approximated by the ideal gas law. The H_2 molecules were initially arranged in a uniform grid within the gas-phase region (Figure 6, left). A rectangular orthorhombic periodic boundary condition was used and the TMA-LiPc molecules were frozen. Each simulation ran for a total of 800 ps with the first 300 ps used to reach equilibrium. System configurations were recorded every 2 ps for the remaining 500 ps for a total of 251 recorded system configurations.

For each system configuration, the percent weight uptake of H_2 in the crystal was calculated and the H_2 molecules in the gas phase were counted to determine the gas-phase pressure. The weight uptake is the ratio of mass of H_2 adsorbed over mass of crystal plus mass of H_2 adsorbed. All H_2 molecules not located within the gas-phase region were assumed to be

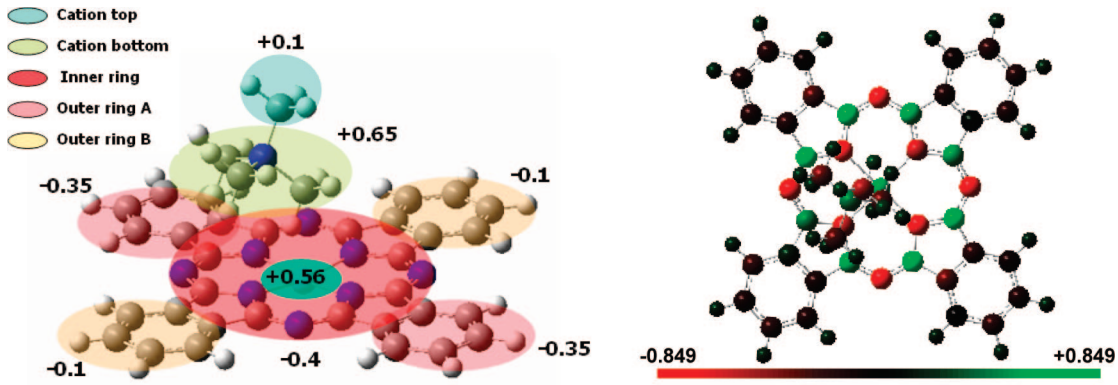

Figure 3. Electrostatic potential (ESP)-derived charges on sites of the TMALiPc molecule calculated with B3LYP/6-31G. Left: Zones of indicated net charge. The green zone inside the inner ring corresponds to the lithium atom. Right: top view of TMA-LiPc with atoms colored according to ESP-fitted charges; color scale shown in the bar.

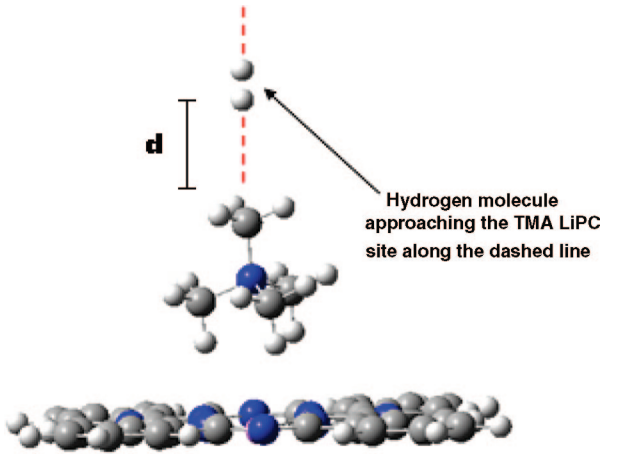

Figure 4. Schematic of H_2 approaching a given site of the TMA-LiPc molecule. H_2 approaches the cation from the top of the molecule. The distance d is changed from 10 to 2.5 Å in a stepwise manner (see text). At each different d, the dipole of the hydrogen molecule is calculated.

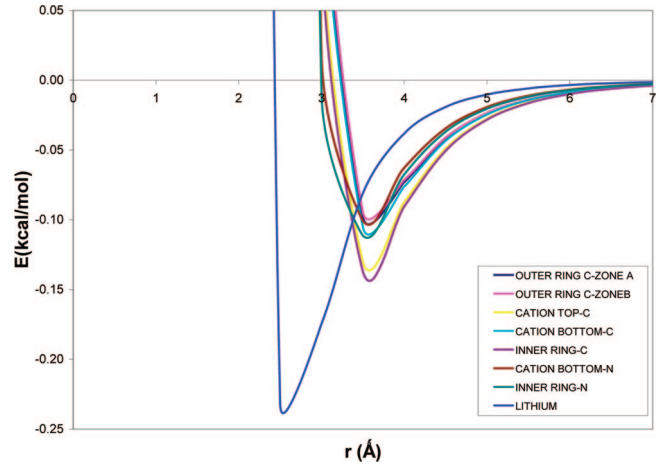

Figure 5. Fitting of LJ + dipole correction data to a LJ function (see text) for different atom types in TMALiPc. The LJ parameters are shown in Table 2.

TABLE 1: Calculated Weight Factor (w_i) According to the Dipole Induced on H_2 from Various TMA LiPc Sites[a]

atom type	$(\mu_i)_{av}$	N_i	S_i	S_i per atom	w_i
outer ring C- zone A	0.06 (0.05)	8	12.87	1.61	0.016
outer ring C- zone B	0.05 (0.05)	8	10.72	1.34	0.013
cation top C	0.15 (0.15)	1	4.02	4.02	0.040
cation C and N	0.08 (0.04)	4	8.58	2.14	0.021
Li	0.14 (0.12)	1	3.75	3.75	0.038
inner ring C	0.17 (0.17)	8	36.46	4.56	0.046
inner ring N	0.11 (0.12)	8	23.59	2.95	0.029

[a] The average induced dipole $(\mu_i)_{av}$ (Debye) on H_2 for each atom type is shown together with the number of atoms of a given type (Ni), and the partial contribution $S_i = (\mu_i N_i / \sum \mu_i N_i) \times 100$. The value in parenthesis in the second column is the average dipole calculated with M05-2X.

TABLE 2: Effective LJ Parameters Used in the MD Simulations for Interaction of Each Atom Type with H_2

atom type in TMA-LiPc	ε (Kcal/mol)	σ (Å)
outer ring A carbon	0.0990	3.162
outer ring B carbon	0.0958	3.170
inner ring carbon	0.1381	3.075
inner ring nitrogen	0.1173	2.990
lithium	0.2553	2.328
cation-top carbon	0.1305	3.090
cation nitrogen	0.1040	3.020
cation-bottom carbon	0.1056	3.145

adsorbed. Each simulation produced a single isotherm point on the pressure-uptake graph representing an average of 251 snapshots.

3. Results

3.1. H_2 Adsorption. Isotherms at two different interlayer separations are shown in Figure 7. The advantage of the larger volume available with the larger ILD separation is significant at low temperatures; for example at 22 bar the H_2 uptake at ILD = 8.49 Å is 6.9 whereas at ILD = 10 Å is 8.3 % wt. At room temperature and low to moderate pressures, the differences in uptakes are less important; however they become significant at higher pressures.

The hydrogen adsorption probability density was estimated from the history file by summing over all configurations the number of hydrogen molecules found within 1 Å of each point of a 3D mesh. The mesh was written out as a Gaussian 98 cube file and visualized with GaussView 3.09. Mesh spacing was 0.33 Bohr to match the Gaussian "coarse" grid spacing option. In order to simplify visualization, hydrogen counts were rounded up to the nearest 10, for example, any points with 11−20 H_2 molecules found near them counted as the same probability density. According to our definition, an x% probability density of H_2 molecules found in a certain region means that the hydrogen molecules spend x% of the time at that region. In all cases (Figures 8−10) we report the regions with the highest probabilities found for a given temperature and pressure, that

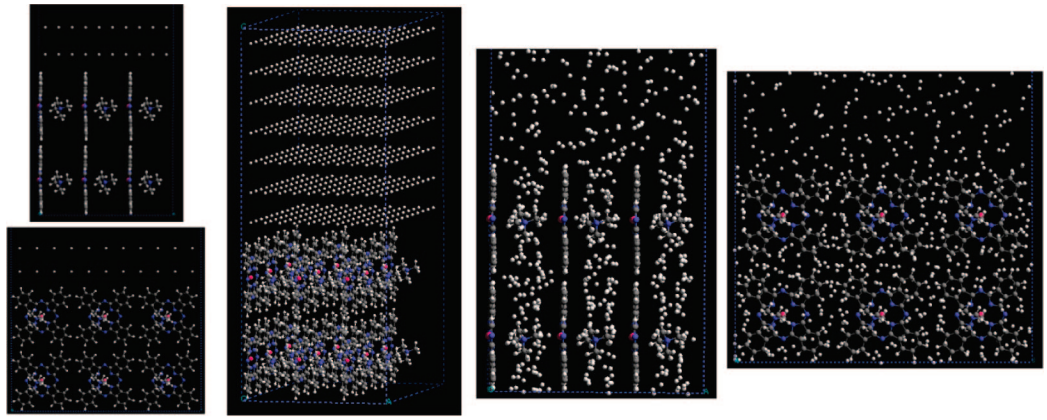

Figure 6. TMA-LiPc initial and final configurations. In the initial configuration, the hydrogen molecules are on the upper part of the simulation cell, arranged in parallel layers. In the final configuration, they are distributed inside the adsorbent phase and also in the gas phase.

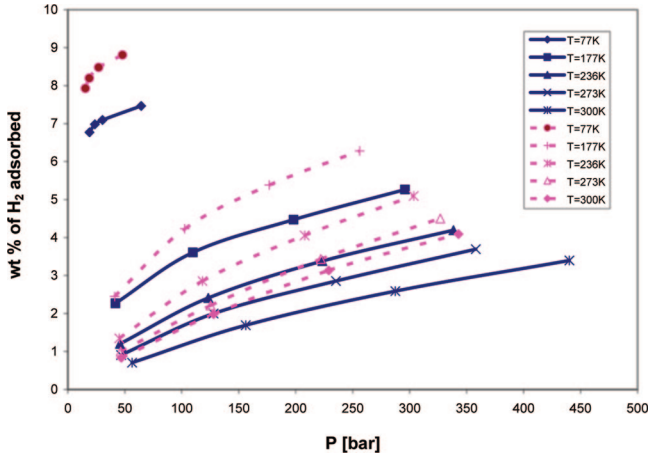

Figure 7. Calculated adsorption isotherms for H_2 in a hypothetical stacked structure of TMA-LiPc at different interlayer distances (ILD): dashed line ILD = 10.0 Å, solid line ILD = 8.49 Å.

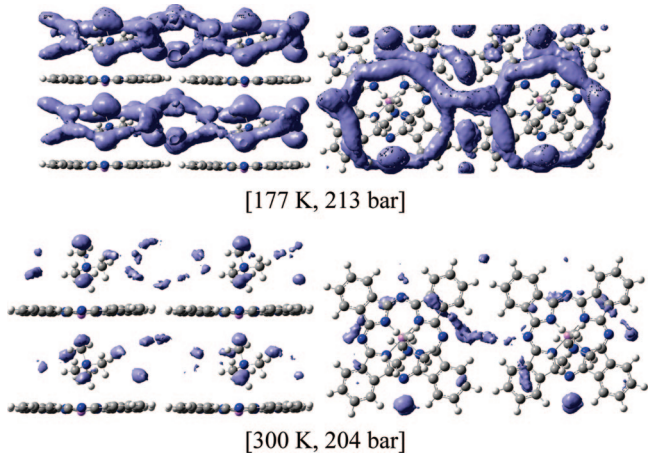

Figure 8. TMA-LiPc H_2 probability surface at ILD 8.49 Å and constant pressure and varying temperature.

is, the strongest adsorption regions; the rest of the time higher kinetic energy molecules are distributed in other regions of the adsorbent space with much lower residence times. The value of the percent is also an indication of the physisorption strength; at high pressures the maximum found was 20%, whereas at lower pressures the maximum probability was only 5%.

Figure 8 shows the 20% H_2 probability densities at the same ILD of 8.49 Å and approximately the same pressure 213 and

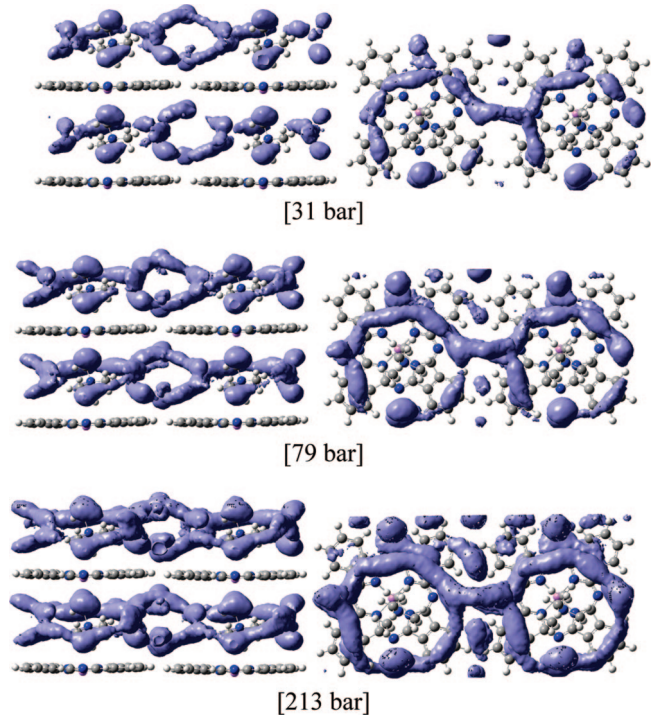

Figure 9. TMA-LiPc H_2 probability surface at ILD 8.49 Å and constant temperature (177 K) and varying pressure.

204 bar, but different temperatures 177 and 300 K. Figure 9 shows the 20% H_2 probability densities at the same ILD (8.49 Å) and temperature (177 K), but at increasing pressures: 31, 79, and 213 bar. Figure 10 shows the 5% H_2 probability densities at the same temperature (300 K), approximately the same pressure (42.65, 42.92 bar) but different ILDs of 8.49 and 10 Å. These figures reveal that as temperature decreases, the high-adsorption region increases (Figure 8), and as pressure increases, the high-adsorption region increases (Figure 9). However, the behavior as ILD increases from 8.49 to 10 Å is different: the high-adsorption region changes shape and splits into two rings separated by about 1.5 Å, each ring closer to a different LiPc anion.

Figures 8 and 9 show that the highest density regions are near the outer ring A carbons, which suggests that the adsorption depends more on the attraction to the outer ring A carbons than it depends on the available space within the crystal. As one compares the H_2 density surfaces from highest to lowest density,

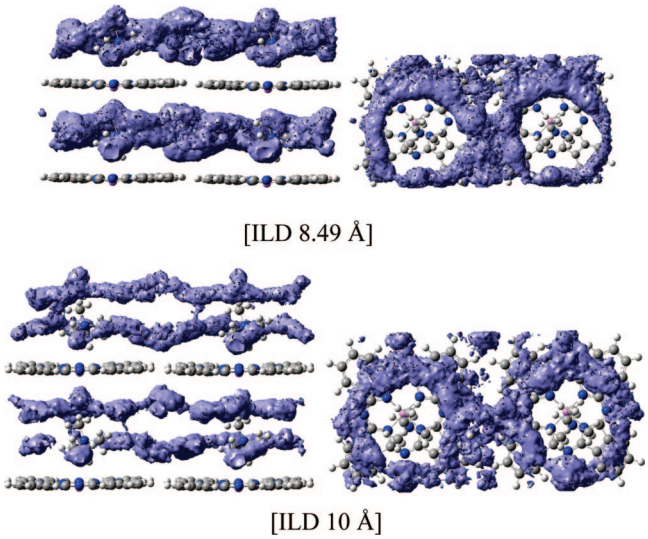

Figure 10. TMA-LiPc H_2 probability surface at constant temperature (300 K), approximately constant pressure, and varying ILD.

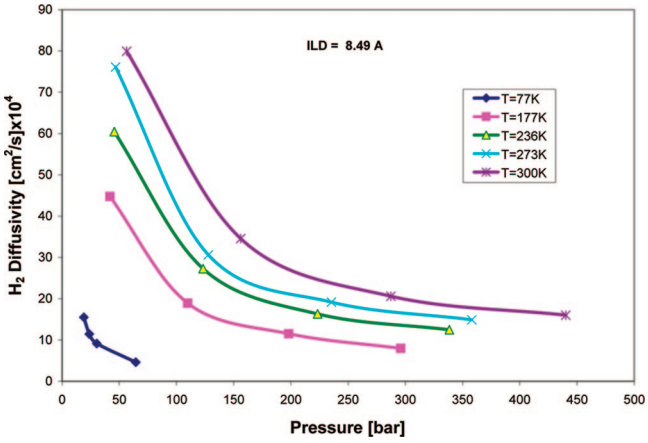

Figure 11. H_2 self-diffusion coefficient at constant ILD of 8.49 Å.

one sees that the H_2 molecules tend to concentrate first near the LiPc anion, then in the large volume between crystal lattice points. Both lower temperatures and higher pressures increase the absolute H_2 density but do not noticeably affect the shape of the H_2 density distribution.

3.2. H_2 Self-Diffusion Coefficient. To better understand the adsorption mechanism, the self-diffusion coefficient of H_2 was estimated from the slope of the mean square displacement (MSD)[21] versus time plot for each MD system. The DL_POLY utility program msdprg.f was used to generate the MSD vs time plots and the slope was fitted by least-squares and converted to a self-diffusion coefficient via

$$D = \frac{\text{slope(MSD)}}{6} \times \left(10^{-8}\frac{\text{cm}}{\text{A}}\right)^2 \times \left(10^{12}\frac{\text{ps}}{\text{s}}\right) \qquad (6)$$

MD systems with the 770 H_2 molecules but lacking the TMA-LiPc crystal were also run to generate gas-only self-diffusion coefficients to compare against. Self-diffusion coefficients at ILD 8.49 Å were compared with those of H_2 gas-only systems (not shown), and it was found that the presence of TMA-LiPc reduces the H_2 diffusion coefficient by 40−90%.[24] Figure 11 shows the isotherms of the H_2 + adsorbent systems at ILD 8.49 Å. At constant low pressures (below approximately 100 bar), there is a dramatic reduction in the diffusion coefficient as temperature decreases. The temperature effect is much less pronounced at higher pressures.

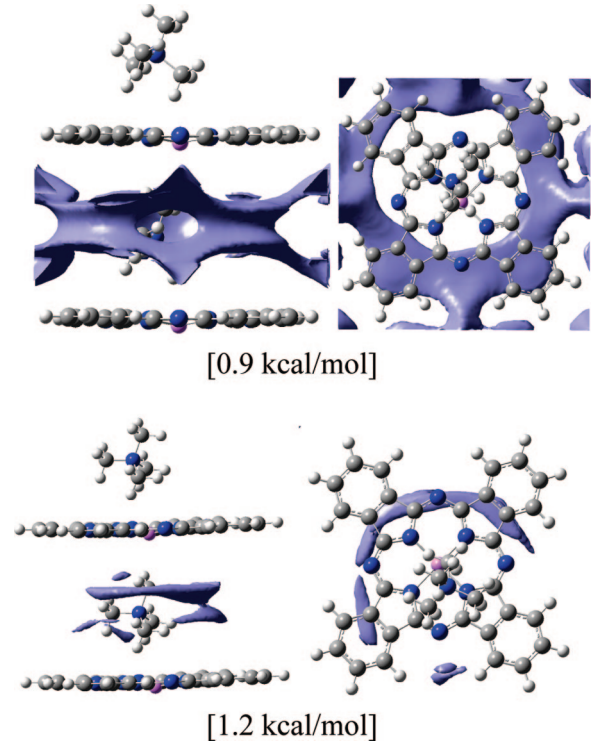

Figure 12. TMA-LiPc H_2 Lennard-Jones binding energy surfaces at ILD 8.49 Å.

3.3. Binding Energy Surfaces. Since the only interatomic potential allowed was due to van der Waals and charge-induced dipole interactions and since the solid adsorbent was fixed in space, it seemed reasonable to expect that the H_2 density profile might be directly predictable by analysis of the binding energy field produced from the MD force field Lennard-Jones parameters. An application was written to generate the binding energy force field from stock DREIDING parameters to test this. Note that these surfaces only show the binding energy from the Lennard-Jones interaction of H_2 and the sites on the macromolecule; the Lennard-Jones interactions of H_2 with H_2 are not computed, yet at high adsorption densities this H_2−H_2 interaction will contribute positively to the total binding energy.

Figure 12 depicts the 0.9 and 1.2 kcal/mol binding energy surfaces for TMA-LiPc at ILD 8.49 Å. Figure 13 shows the 0.9 and 1.2 kcal/mol binding energy surfaces for TMA-LiPc at ILD 10 Å. These surfaces closely mirror the actual H_2 density profiles portrayed in Figures 8 through 10, including the splitting of the high density region at ILD 10 Å. These figures appear to directly correlate quite well to the high-density region in the H_2 probability surfaces. As in the H_2 density graphs (Figure 10 at 10 Å separation), the 0.9 kcal/mol binding region splits at ILD 10 Å; thus it can be concluded that the shape of the H_2 density profile follows that of the strongest binding energies. Looking down at the 0.9 kcal/mol images, one sees protrusions along the centers of the rings around the cation above the void spaces between the outer phenyl groups on the Pc.

Figures 12 and 13 suggest that the high-density portions of the H_2 probability surfaces can be predicted and do visibly correlate with the actual structure of the adsorbed H_2, but they do not by themselves directly predict the total adsorption. One possible reason for this is that the binding energy drives the adsorption only near the atoms of the macromolecule; in the larger void spaces of the crystal the binding energy is negligible.

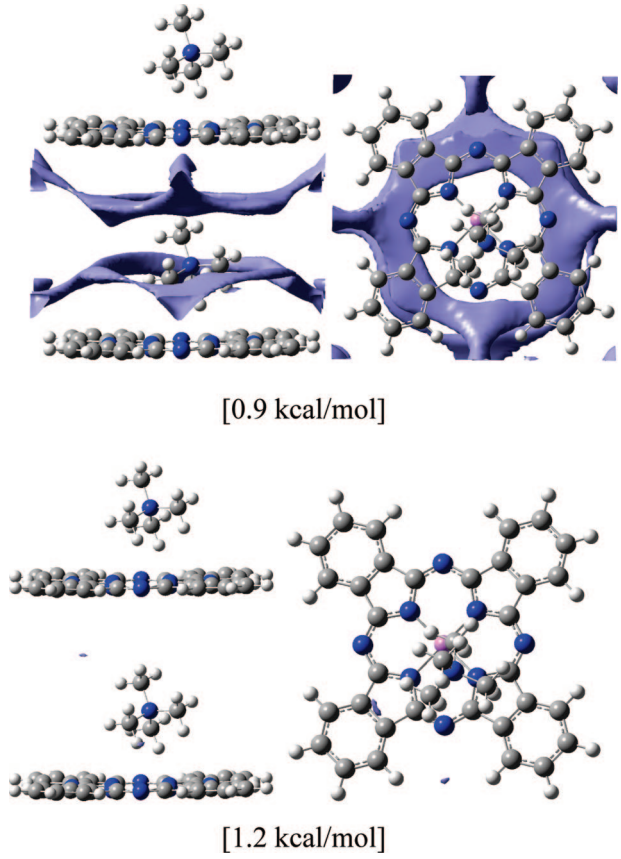

Figure 13. TMA-LiPc H_2 Lennard-Jones binding energy surfaces at ILD 10 Å.

The void volume thus must somehow be taken into account before the total adsorption could be predicted.

4. Conclusions

The adsorbed H_2 probability density lends support to the idea that the H_2 adsorption is more a function of attraction to the LiPc anion rather than available space within the crystal. If true, this also means that adsorption isotherms estimated from the MD might be accurate even if the MD simulations were based on an incorrect crystal structure. However, the comparison of the strongest probability density regions with the strongest binding energy regions suggests that the available volume also plays a significant role in the total adsorption, even though part of the H_2 molecules are distributed in regions of much lower binding energy. The high percent of H_2 storage found at low temperatures (177 K) and moderate pressures (50 to 100 bar) indicates that further investigation of materials with large dipoles is certainly warranted. We also emphasize that there is a benefit for having a layered structure which predicts more wt % H_2 adsorbed than just what one would expect based on doubling the binding energy of the adsorbent due to co-operative interaction as discussed in our previous paper on corannulene. Ab initio calculated results for the change in Gibbs energy suggest that the effect of a layered structure is to reduce the binding energy requirements for a reaction to be thermodynamically allowed. These results are being prepared for publication in a separate manuscript.

The MD calculated adsorption of H_2 using only one layer of TMA-LiPc yields 0.72 wt % at 75 bar and 298 K; this value is approximately 74% larger at the same conditions when we assume the layered structure at the larger separation (10 Å) which allows for cooperative interactions (see results in Figure 7). Experimentally it was found that 0.72 wt % H_2 is adsorbed at 298 K and 75 bar in the higher-molecular weight TBA-LiPc; thus allowing for the difference in molecular weight, we should expect approximately 0.92 wt % for adsorption in TMA-LiPc, which is in fair agreement with the calculated values of 0.72 wt % calculated for the monolayer and 0.9 for the layered structure. This also suggests that it is the complex anion which is primarily involved in the adsorption process with molecular hydrogen. The purpose of the tetra-alkyl-ammonium cation is merely to provide access for hydrogen adsorption on both sides of the phthalocyanine complex anion and spacing between the phthalocyanine rings.

Acknowledgment. This work is supported by funds from the Air Force Research Laboratory. Supercomputer time provided by the TAMU supercomputer center and by the DoD Major Shared Resource Centers (ARL MSRC and ASC MSRC) is gratefully acknowledged.

Supporting Information Available: Structures of TMA Li-Pc monomer calculated with B3LYP/6-31 g(d,p), B3LYP/g-31 g(d,p)++, and M05-2X/6-31 g(d,p), as well as those of the dimer calculated with B3LYP/6-31 g(d,p) and M05-2X/6-31 g(d,p) are included. This material is available free of charge via the Internet at http://pubs.acs.org.

References and Notes

(1) Zuttel, A. Materials for hydrogen storage. *Mater. Today* **2003**, *6*, 24–33.

(2) Scanlon, L. G.; Balbuena, P. B.; Zhang, Y.; Sandi, G.; Back, C. K.; Feld, W. A.; Mack, J.; Rottmayer, M. A.; Riepenhoff, J. L. Investigation of corannulene for molecular hydrogen storage via computational chemistry and experimentation. *J. Phys. Chem. B* **2006**, *110*, 7688–7694.

(3) Zhang, Y.; Scanlon, L. G.; Balbuena P. B. Hydrogen Adsorption in Corannulene-Based Materials. In *Nanomaterials: Design and Simulation*; Balbuena, P. B., Seminario, J. M., Eds.; Elsevier Science Publishers: Amsterdam, 2006; Vol. 18; pp 127−166.

(4) Zhang, Y.; Scanlon, L. G.; Rottmayer, M. A.; Balbuena, P. B. Computational investigation of adsorption of molecular hydrogen on lithium-doped corannulene. *J. Phys. Chem. B* **2006**, *110*, 22532–22541.

(5) Lochan, R. C.; Head-Gordon, M. Computational studies of molecular hydrogen binding affinities: The role of dispersion forces, electrostatics, and orbital interactions. *Phys. Chem. Chem. Phys.* **2006**, *8*, 1357–1370.

(6) Grossie, D. A.; Feld, W. A.; Scanlon, L.; Sandi, G.; Wawrzak, Z. Di-acetone-2O:O-bis[(acetone-O)aqualithium(I)] di-acetone-2O:O-bis[di-aqualithium(I)] tetrakis{[phthalocyaninato(2-)-4N,N′,N″,N‴]lithiate(I)}. *Acta Cryst. E* **2006**, *62*, m827–m829.

(7) Zhang, Y.; Alonso, P. R.; Martinez-Limia, A.; Scanlon, L. G.; Balbuena, P. B. Crystalline structure and lithium-ion channel formation in self-assembled di-lithium phtalocyanine: Theory and experiments. *J. Phys. Chem. B* **2004**, *108*, 4659–4668.

(8) Becke, A. D. Density-functional thermochemistry. III. The role of exact exchange. *J. Chem. Phys.* **1993**, *98*, 5648–5652.

(9) Becke, A. D. A new mixing of Hartree-Fock and local density-functional theories. *J. Chem. Phys.* **1993**, *98*, 1372–1377.

(10) Lee, C.; Yang, W.; Parr, R. G. Development of the Colle-Salvetti correlation-energy formula into a functional of the electron density. *Phys. Rev. B* **1988**, *37*, 785–789.

(11) Schreiner, P. R.; Fokin, A. A.; Pascal, R. A.; deMeijere, A. Many density functional theory approaches fail to give reliable large hydrocarbon isomer energy differences. *Org. Lett.* **2006**, *8*, 3635–3638.

(12) Wodrich, M. D.; Corminboeuf, C.; Schleyer, P. V. Systematic errors in computed alkane energies using B3LYP and other popular DFT functionals. *Org. Lett.* **2006**, *8*, 3631–3634.

(13) Sagara, T.; Ganz, E. Calculations of dihydrogen binding to doped carbon nanostructures. *J. Phys. Chem. C* **2008**, *112*, 3515–3518.

(14) Denis, P. A. Investigation of H2 physisorption on corannulene (C20H10), tetraindenocorannulene (C44H18), pentaindenocorannulene (C50H20), C60, and their nitrogen derivatives. *J. Phys. Chem. C* **2008**, *112*, 2791–2796.

(15) Zhao, Y.; Schultz, N. E.; Truhlar, D. G. Design of Density Functionals by Combining the Method of Constraint Satisfaction with Parametrization for Thermochemistry, Thermochemical Kinetics, and Noncovalent Interactions. *J. Chem. Theory Comput.* **2006**, *2*, 364–382.

(16) Frisch, M. J. ; Trucks, G. W.; Schlegel, H. B.; Scuseria, G. E.; Robb, M. A.; Cheeseman, J. R.; Montgomery, J. A.; Vreven, T.; Kudin, K. N. ; Burant, J. C.; Millam, J. M.; Iyengar, S. S.; Tomasi, J.; Barone, V.; Mennucci, B.; Cossi, M.; Scalmani, G.; Rega, N.; Petersson, G. A.; Nakatsuji, H.; Hada, M.; Ehara, M.; Toyota, K.; Fukuda, R.; Hasegawa, J.; Ishida, M.; Nakajima, T.; Honda, Y. ; Kitao, O.; Nakai, H.; Klene, M.; Li, X.; Knox, J. E.; Hratchian, H. P.; Cross, J. B.; Bakken, V.; Adamo, C.; Jaramillo, J.; Gomperts, R.; Stratmann, R. E.; Yazyev, O.; Austin, A. J.; Cammi, R.; Pomelli, C.; Ochterski, J. W.; Ayala, P. Y.; Morokuma, K.; Voth, G. A.; Salvador, P.; Dannenberg, J. J.; Zakrzewski, V. G.; Dapprich, S.; Daniels, A. D.; Strain, M. C.; Farkas, O.; Malick, D. K.; Rabuck, A. D.; Raghavachari, K.; Foresman, J. B.; Ortiz, J. V.; Cui, Q.; Baboul, A. G.; Clifford, S.; Cioslowski, J.; Stefanov, B. B.; Liu, G.; Liashenko, A.; Piskorz, P.; Komaromi, I.; Martin, R. L.; Fox, D. J.; Keith, T.; Al-Laham, M. A.; Peng, C. Y.; Nanayakkara, A.; Challacombe, M.; Gill, P. M. W.; Johnson, B.; Chen, W.; Wong, M. W.; Gonzalez, C.; Pople, J. A. *Gaussian03*, Revision C.02 ed.; Gaussian, Inc.: Wallingford, CT, 2004.

(17) Prausnitz, J. M.; Lichtenthaler, R. N.; deAzevedo, E. G. *Molecular Thermodynamics of Fluid Phase Equilibria*, 3rd ed.; Prentice Hall: NJ, 1999.

(18) Gray, C. G.; Gubbins, K. E. *Theory of Molecular Fluids*; Clarendon Press: Oxford, 1984; Vol. 1.

(19) Besler, B. H.; Merz, K. M.; Kollman, P. A. Atomic Charges Derived from Semiempirical Methods. *J. Comput. Chem.* **1990**, *11*, 431–439.

(20) Mayo, S. L.; Olafson, B. D.; Goddard, W. A. Dreiding: A generic force field for molecular simulations. *J. Phys. Chem.* **1990**, *94*, 8897–8909.

(21) Allen, M. P.; Tildesley, D. J. *Computer Simulation of Liquids*; Oxford University Press: Oxford, 1990.

(22) Evans, D. J.; Morriss, G. P. The isothermal/isobaric molecular dynamics ensemble. *Phys. Lett.* **1983**, *98A*, 433–436.

(23) Smith, W.; Forester, T. R. DL_POLY_2.0: A general-purpose parallel molecular dynamics simulation package. *J. Mol. Graphics* **1996**, *14*, 136–141.

(24) Lamonte, K. Modeling H_2 adsorption in carbon-based structures. M.Sc. Thesis, Texas A&M University, College Station, TX, 2008.

JP8050998